Numerical Simulation of Rarefied Nozzle Plume Impingements

Toru Hyakutake and Michio Nishida

Department of Aeronautics and Astronautics, Kyushu University
Fukuoka 812-8581, Japan

Abstract. This paper describes numerical simulation of rarefied nozzle plume impingements. Two different reservoir pressures 400 kPa and 4 kPa are considered. In the case of 400 kPa, the simulation of the nozzle flow was conducted by using the Navier-Stokes equation, and then the analysis of the plume flow was carried out by the DSMC method, employing the nozzle exit conditions obtained by Navier-Stokes equation. On the other hand, for 4 kPa, both the nozzle flow and the plume impingement have been calculated using the DSMC method. Concerning the angle between the nozzle axis and the flat plate, three kinds of angle are selected, that is, 90°, 45° and 0°. In addition, we considered the case where there exists a flat plate behind the nozzle. Simulated results have been compared with the existing experiments for the pressure and shear stress distributions on the flat plate. A good agreement between the DSMC results and the experiments are shown. In the case of the oblique and parallel impingements, the location of the impingement pressure peak and the stagnation point shifted upstream with increasing rarefaction.

INTRODUCTION

Satellites and spacecrafts are usually equipped with thrusters for attitude control. Exhaust gas from the thruster expands into the space vacuum and generates a huge plume in the space. As a result, the plume may impinge on the satellite body, antennas or solar panels. This impingement causes significant problems of surface degradation, contamination, heat loads, disturbance torque and so forth. Hence, it is worth while investigating the detailed structure of the plume impingement for the purpose of space engineering.

The flat plate impingements of a nozzle plume have been experimentally examined by Legge [1] in a high vacuum facility. He measured pressure and shear stress on a flat plate for normal and oblique impingements, and compared with the impingement model [2] based on Simon's plume model [3]. Concerning the numerical simulation, the direct simulation Monte Carlo (DSMC) method introduced by Bird [4] has been widely used in rarefied gas flows with the development of computers. The problem of the nozzle plume impingement on a perpendicular surface has been studied by using the DSMC method [5]. However, there are no numerical studies concerning parallel and oblique impingements on a flat plate.

Figure 1 illustrates several types of a nozzle plume impingement, where β is the angle between the nozzle axis and the flat plate and θ_{lim} the maximum turning angle of a stream line at the nozzle exit. The model field means the area where Simon's plume model is applicable. The model field is dependent on the angle θ_{lim}. Therefore, there exists the area where the impingement model is not available, especially in the cases of (c) and (d). In the present paper, we have performed the numerical simulation of nozzle plume impingements on a flat plate, and calculated the impingement pressure in the area where the impingement model is not applicable. In the case of the normal and oblique impingements, we also compared quantitatively with Legge's experimental data for the pressure and the shear stress distributions on the flat plate.

NUMERICAL METHOD

A plume impingement considered in the present study is such that gas is expanded through a nozzle into vacuum and then interacts with a flat plate. The diameters of the nozzle throat and the nozzle exit are 0.6 mm

CP585, *Rarefied Gas Dynamics: 22nd International Symposium,* edited by T. J. Bartel and M. A. Gallis

Report Documentation Page

Report Date	Report Type	Dates Covered (from... to)
09JUL2000	N/A	-

Title and Subtitle Numerical Simulation of Rarefied Nozzle Plume Impingements	**Contract Number**
	Grant Number
	Program Element Number
Author(s)	**Project Number**
	Task Number
	Work Unit Number
Performing Organization Name(s) and Address(es) Department of Aeronautics and Astronautics, Kyushu University Fukuoka 812-8581, Japan	**Performing Organization Report Number**
Sponsoring/Monitoring Agency Name(s) and Address(es) AOARD Unit 45002 APO AP 96337-5002	**Sponsor/Monitor's Acronym(s)**
	Sponsor/Monitor's Report Number(s)

Distribution/Availability Statement
Approved for public release, distribution unlimited

Supplementary Notes
Papers from Rarefied Gas Dynamics (RGD) 22nd International Symposium held in Sydney, Australia on 9-14 July 2000. See also ADM001341 for whole conference on cd-rom.

Abstract

Subject Terms

Report Classification unclassified	**Classification of this page** unclassified
Classification of Abstract unclassified	**Limitation of Abstract** UU

Number of Pages
6

and 4.75 mm, respectively. The nozzle length is 7.75 mm and the nozzle-divergent angle is 30°. In Figs. 2, 3 and 4, the computational fields for Fig. 1 (a), (c) and (d) are shown, respectively. The numerical simulations for the reservoir pressure P_0=400 kPa (case 1) and 4 kPa (case 2) are conducted in the present paper. For case 1, the continuum theory is applicable inside the nozzle. Hence, we simulated the nozzle flow by using the Navier-Stokes equation. DSMC simulation of the plume flow is carried out by using the nozzle exit conditions obtained by Navier-Stokes simulation. On the other hand, for case 2, both the nozzle flow and the plume impingement have been calculated using the DSMC method. In the cases of Figs. 2 and 3, the distance between the flat plate and the center of the nozzle exit L is set to 40 mm in order to compare the simulation with Legge's experiments. Two different distances of L are selected in Fig. 4, 0 mm and 15.5 mm.

In the present calculation, nitrogen was adopted as a test gas to compare with Legge's experiments. The flowfield model considered here is such that molecules impinging on a flat plate suffer diffuse reflection, and the temperature on the flat plate is assumed as equal to laboratory temperature (300K). Molecules across the symmetric plane suffer specular reflection. Outflow conditions are used as ambient conditions. Collisions of molecules are simulated using the variable hard sphere (VHS) model [6]. The Borgnakke-Larsen statistical model [7] is employed for the calculation of the energy exchange between translational and rotational modes, together with temperature-dependent energy exchange probability of Boyd [8]. The computational domain consists of 9 to 14 subregions for efficient computations, with total cells of 405,300. The total number of simulated molecules in this domain is 9.0×10^5 in the case of the oblique impingement (case 1).

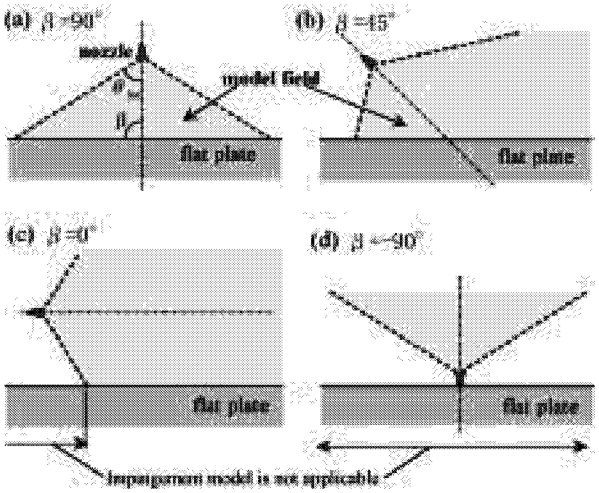

FIGURE 1. Impingement types

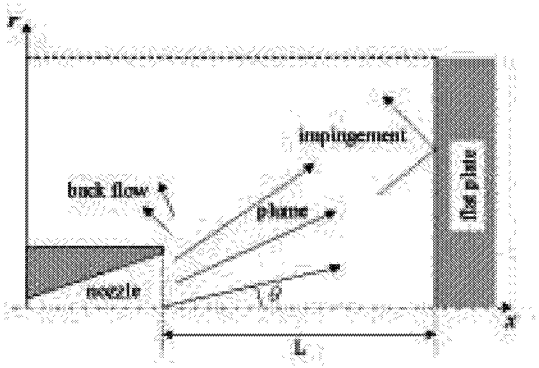

FIGURE 2. Computational field for Fig. 1 (a)

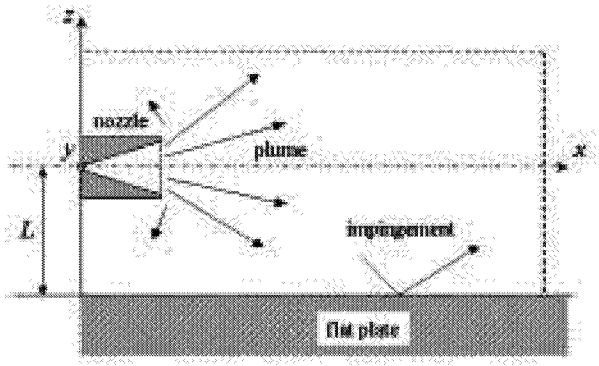

FIGURE 3. Computational field for Fig. 1 (c)

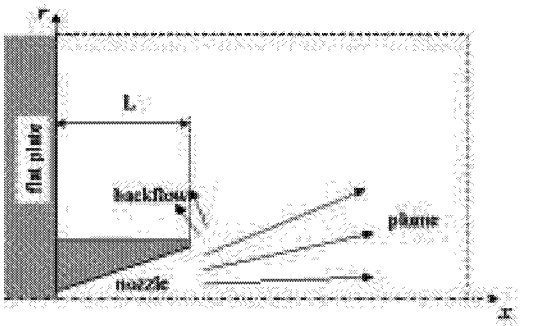

FIGURE 4. Computational field for Fig. 1 (d)

RESULTS AND DISCUSSION

First, the numerical simulation of a nozzle plume is conducted without considering the flat plate. Figures 5 and 6 show translational temperature and number density contours for case 1 in the nozzle and the vicinity of the nozzle exit. At the center of the nozzle exit, Mach number is 5.8, the temperature is 39 K and the Knudsen number is 1/2087. It is difficult to make the cell of the mean free path length because the vicinity of nozzle exit is still a continuum flow. In the present DSMC simulation, therefore, the cell which is larger than the mean free path length was employed near the nozzle exit. In Figs. 7 and 8, translational temperature and number density contours for case 2, respectively, are illustrated. The nozzle flow simulation for case 2 indicates that Mach number is 3.9, translational temperature is 74 K and the Knudsen number is 1/60 at the center of the nozzle exit. As the reservoir pressure is decreased, the nozzle flow is influenced by the nozzle wall and the boundary layer becomes large. Comparison of Fig. 6 with Fig. 8 shows that the backflow of the nozzle plume for case 2 is more significant than that for case 1.

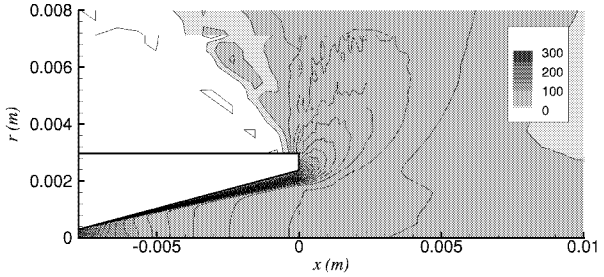

FIGURE 5. Translational temperature contours for case 1

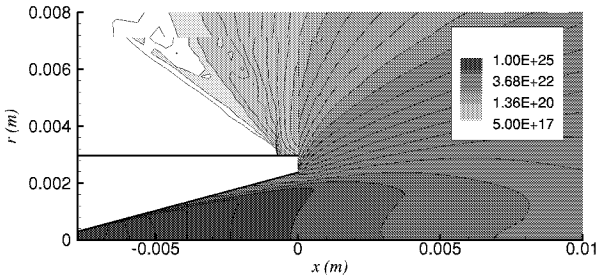

FIGURE 6. Number density contours for case 1

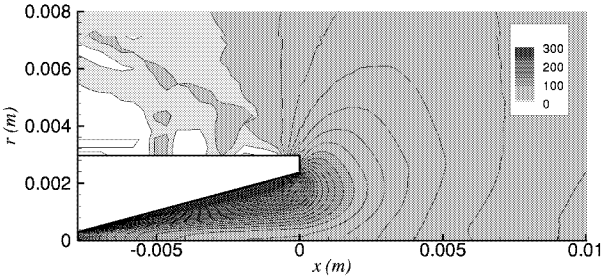

FIGURE 7. Translational temperature contours for case 2

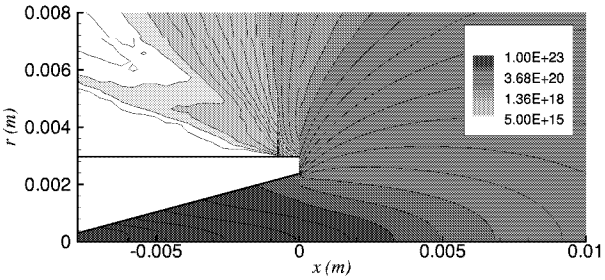

FIGURE 8. Number density contours for case 2

Figure 9 shows the comparison between the simulation and experiments of the pressure distribution on the flat plate for the normal impingement ($\beta = 90°$). As shown in this figure, there is an excellent agreement between the simulation and the experiments for the impingement pressure distributions. It is indicated that the DSMC method is valid to simulate the nozzle plume impingement by using the nozzle exit conditions from the Navier-Stokes solution, in spite of large cell near the nozzle exit. In the present paper, the numerical simulation for the more rarefied conditions than case 1 is conducted to investigate the effect of the rarefaction, this is case 2. Comparison between case 1 and case 2 is also illustrated in Fig. 9. Inside the nozzle, for case 2, the flow is already rarefied, therefore, Mach number at the nozzle exit for case 2 is smaller than that for case 1. As a result, it is seen that the impingement pressure for case 2 is smaller than that for case 1. Figure 10 shows the comparison between the DSMC results and Legge's experiments for the shear stress distributions on the flat plate. The present result shows a good agreement with Legge's experiments. The minimum of the impingement shear stress ($x/L = 0$) means the location of the stagnation point. For case 2, the maximum of the calculated results is slightly smaller than that of case 1.

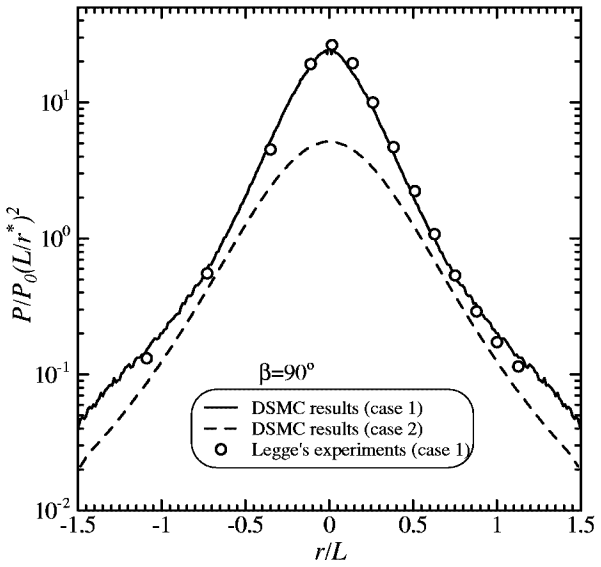

FIGURE 9. Pressure distributions on the flat plate for $\beta = 90°$

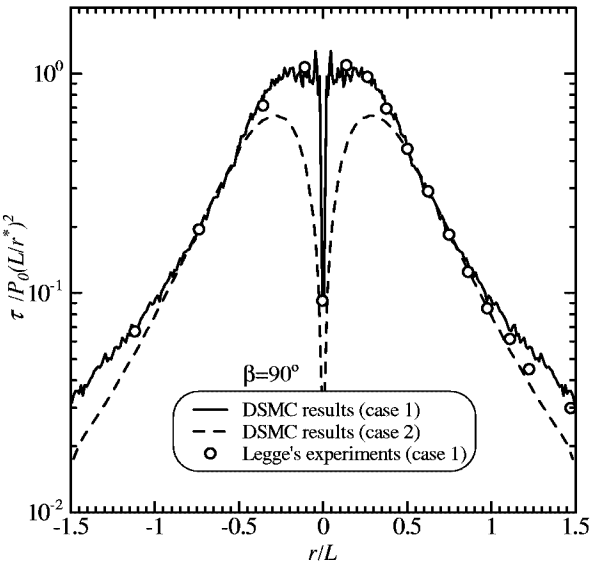

FIGURE 10. Shear stress distributions on the flat plate for $\beta = 90°$

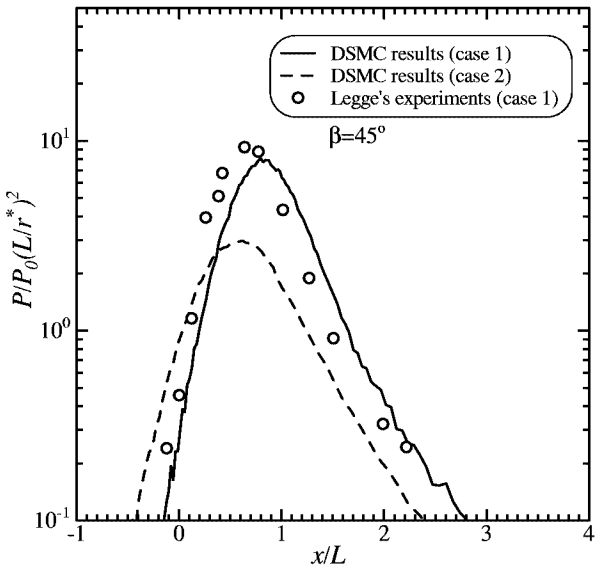

FIGURE 11. Pressure distributions on the flat plate for $\beta = 45°$

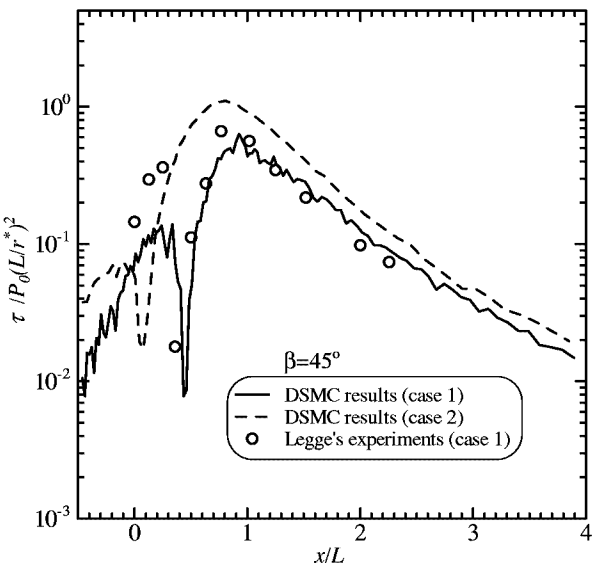

FIGURE 12. Shear stress distributions on the flat plate for $\beta = 45°$

In the case of the oblique impingement, the angle between the nozzle axis and the flat plate is 45°. Figure 11 illustrates the comparison between the DSMC results and the experiments for the impingement pressure. As shown in this figure, the DSMC result for case 1 indicates the feature similar to the experiments. Comparison between case 1 and case 2 shows the location of pressure peak is shifted upstream on the plate with increasing rarefaction in case 2. Figure 12 shows the comparison for the shear stress. The DSMC result for case 1 indicates a good agreement with the experimental data at $x/L > 0.45$. It is seen that the location of the stagnation point is between $x/L = 0$ and the location of the corresponding impingement pressure peak, that is $x/L = 0.45$ for case 1 and $x/L = 0.05$ for case 2, respectively. Unlike the normal impingement, the maximum of the impingement shear stress become large, as the reservoir pressure is decreased.

Next, we consider the parallel impingement. Figure 13 shows the comparison between case 1 and case 2 for

the impingement pressure distributions. Experimental data for the parallel impingement don't exist, so that the comparison of the simulation with the experiment is not shown in the present paper. As the reservoir pressure is decreased, the maximum of the impingement pressure shifts upstream on the plate. That means the expansion of the nozzle plume is large with increasing rarefaction. In the case of the oblique and normal impingement, the maximum of the impingement pressure for case 2 was smaller than that for case 1. In the case of the parallel impingement, on the other hand, the maximum of the pressure for case 2 is larger than that for case 1. In Fig. 14, the comparison for the impingement shear stress distribution is illustrated. The shear stresses for case 2 is larger than those for case 1.

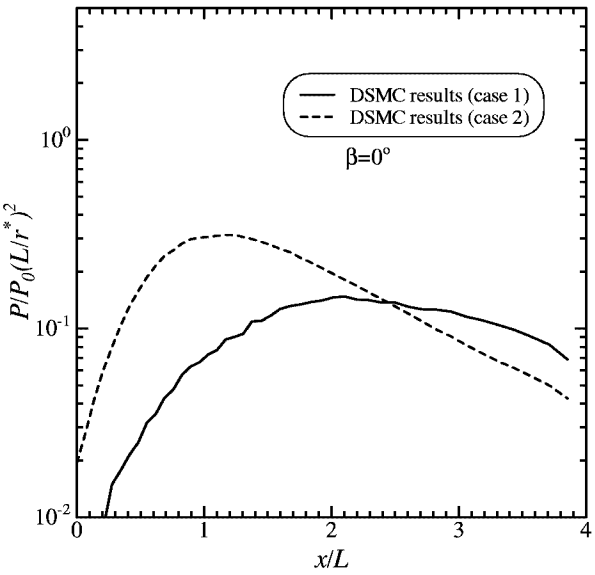

FIGURE 13. Pressure distributions on the flat plate for $\beta = 0°$

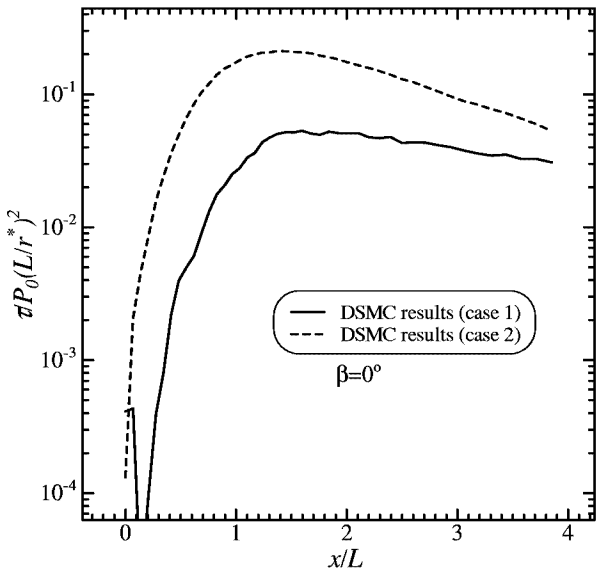

FIGURE 14. Shear stress distributions on the flat plate for $\beta = 0°$

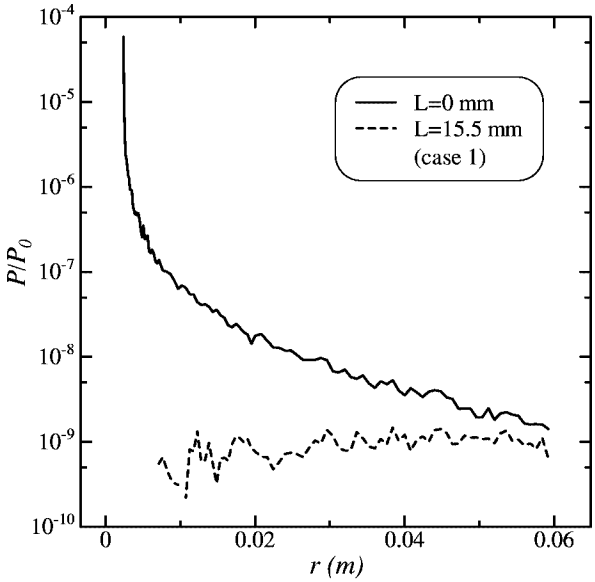

FIGURE 15. Pressure distributions on the flat plate for $\beta = -90°$ (case 1)

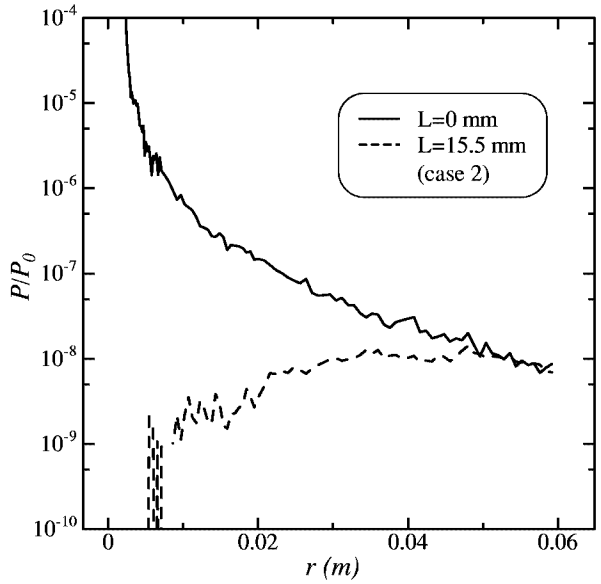

FIGURE 16. Pressure distributions on the flat plate for $\beta = -90°$ (case 2)

Finally, we simulated the case that there exists the flat plate behind the nozzle (Fig. 4). We consider $L = 0$

mm and 15.5 mm as the distance between the nozzle axis and the flat plate. Figure 15 shows the impingement pressure on the flat plate for case 1. The maximum of the impingement pressure is at the edge of the nozzle ($r = 2.375$ mm) in the case of $L = 0$ mm, and the pressure is decreased as away the nozzle. However, the pressure on the flat plate for $L = 15.5$ mm is almost constant, 1.0×10^{-9}. There doesn't exist the impingement pressure at 0 mm $< r <$ 0.007 mm, because molecules in the DSMC simulation don't exist in the area outside the expansion angle. The comparison of two results illustrated that the impingement pressure for $L = 0$ mm and 15.5 mm approach the value $P/P_0 = 1.0 \times 10^{-9}$ away from the nozzle. In Fig. 16, the impingement pressure for case 2 is illustrated. The comparison of Fig. 15 with Fig. 16 shows that the impingement pressure for case 2 is larger than that for case 1, because the number of molecules scattering behind the nozzle is increased, as the reservoir pressure is decreased. The pressures for both $L = 0$ mm and 15.5 mm approach the value $P/P_0 = 1.0 \times 10^{-8}$, away from the nozzle.

CONCLUSIONS

The DSMC simulation of normal, oblique ($\beta = 45°$) and parallel nozzle plume impingements on a flat plate yielded the following conclusions: By combining the Navier-Stokes equation with the DSMC method, the numerical simulation of the nozzle plume impingement was conducted. The calculated results were compared with the Legge's experiments for pressure and shear stress distributions on the flat plate, and a good agreement between two results was obtained. It may be mentioned, therefore, that the DSMC method is valid to simulate the nozzle plume impingement by using the nozzle exit conditions from the Navier-Stokes solution. In the case of the parallel impingement, it is seen that the normalized impingement pressure and shear stress become large with increasing rarefaction. In addition, the simulation of the case that there exists the flat plate behind the nozzle (Fig. 4) is conducted. It was revealed that the impingement pressure approaches a value away from the nozzle independently of the distance between the nozzle exit and the flat plate.

REFERENCES

1. Legge, H., *Plume Impingement Forces on Inclined Flat Plate*, Rarefied Gas Dynamics, pp.955-962, 1990.
2. Legge, H., *Plume Impingement on Inclined Flat Plates in Continuum and Rarefied Flow,*
   Part 1: Flow Survey by Glow Discharge and Liquid Crystal Surface Temperature Visualization, DFVLR-IB 222 88 A 02, 1988.
   Part 2: Experimental Wall Shear Stress and Pressure Distributions, DFVLR-IB 222-88 A 03, 1988.
   Part 3: Modelling of Wall Shear Stress and Pressure Distributions, DFVLR-IB 222-88 A 04, 1988.
3. Simon, G.A., *Effect of Nozzle Boundary Layers on Rocket Exhaust Plumes*, AIAA J., **10** (1972), pp.1534-1535
4. Bird G.A., *Molecular Gas Dynamics and the Direct Simulation of Gas Flows*, Clarendon Oxford, 1994.
5. Kim, B.G. and Soga, T., *Numerical Simulation of Impingement of Free Jet into a Vacuum from a Supersonic Nozzle on a Perpendicular Flat Plate*, Proceeding of International Symposium of Aerospace and Fluid Dynamics, Nov. 14-16, pp.564-571, 1993.
6. Bird G.A., *Monte-Carlo Simulation in an Engineering Context*, Progress in Astronautics and Aeronautics, Vol.74, pp.239-255, AIAA, 1981.
7. Borgnakke, C. and Larsen, P. S., *Statistical Collision Model for Monte Carlo Simulation of Polyatomic Gas Mixture*, J. Comput. Phys., **18** (1975), pp.405-420.
8. Boyd, I.D., *Analysis of Rotational Nonequilibrium in Standing Shock Waves of Nitrogen*, AIAA J., **28** (1990), pp.1997-1999.